PROGRESS IN WEAK FLUID-STRUCTURE-COUPLING FOR MULTIBLADED ROTORS IN HIGH-SPEED FORWARD FLIGHT

Klausdieter Pahlke
DLR, Institute of Aerodynamics and Fluid Technology
D-38108 Braunschweig, Lilienthalplatz 7
email: Klausdieter.Pahlke@dlr.de

Berend van der Wall
DLR, Institute of Flight Research
D-38108 Braunschweig, Lilienthalplatz 7
email: Berend.vanderWall@dlr.de

Abstract: Progress in coupling the DLR rotor simulation code S4 and the DLR Navier-Stokes solver FLOWer following a weak coupling approach is reported. The method allows to produce trimmed CFD solutions for rotors in high-speed forward flight with inclusion of elastic blade deformations and viscous effects. The weak coupling procedure is applied to high-speed forward flight test cases of the 7A and the 7AD rotor. Isolated blade computations are carried out for both rotors while the full 4-bladed rotor is simulated only in the 7A case using the chimera approach. The weak coupling which includes the transfer of normal forces (c_n), tangential forces (c_t) and pitching moments (c_m) from the CFD code to the rotor simulation code improved the agreement with the existing experimental data compared to the uncoupled computations considerably. The performance difference between the 7A and the 7AD rotor in high-speed forward flight is well predicted.

Nomenclature:

a_∞	free stream speed of sound
b	number of blades
c	local blade chord
c_mM^2	local pitching moment coefficient ($P/(0.5\rho_\infty a_\infty^2 c^2$ unit length))
c_nM^2	local normal force coefficient ($N/(0.5\rho_\infty a_\infty^2 c$ unit length))
c_tM^2	tangential force coefficient ($T/(0.5\rho_\infty a_\infty^2 c$ unit length))
M	local reference Mach number
M_∞	free stream Mach number
$M_{\omega R}$	Mach number due to rotational motion of the blade tip ($\omega R/a_\infty$)
N	normal force [N]
P	pitching moment [Nm]
r	radial coordinate [m]
R	rotor radius [m]
T	tangential force [N]
Xb	non-dimensional propulsive force (see definition of Zb)
y+	non-dimensional distance normal to the blade surface
Zb	non-dimensional lift force =100*liftforce/($0.5\rho_\infty$ *b*c_{root}*R*(ωR)2)
α_q	rotor shaft angle [^{o}]
β	flapping angle [^{o}] $\beta=\beta_0+\beta_S\sin(\psi)+\beta_C\cos(\psi)+.....$
μ	advance ratio ($M_\infty/ M_{\omega R}$)
ϑ	elastic torsion angle [^{o}]
θ	pitch angle [^{o}], $\theta=\theta_0+\theta_S\sin(\psi)+\theta_C\cos(\psi)$
θ_0	collective pitch angle [^{o}]
θ_C	lateral pitch angle [^{o}]
θ_S	longitudinal pitch angle [^{o}]
ψ	azimuth angle [^{o}]
ω	rotational angular velocity [1/s]

Introduction

Because of their unique hovering capability helicopters are playing a more and more important role in our society. Their missions range from military applications, law enforcement to save and rescue applications. In spite of this obvious success today's helicopters still suffer from a number of technical weaknesses and shortcomings reducing their ability to fulfill new potential roles and to match society expectations (see [1]). Therefore the major aerodynamic goals of the helicopter industry are to extend the flight envelope, to improve the performance and to reduce the noise of helicopters. In order to reach these goals new design tools are needed which are much more accurate and reliable than today's industrial tools.

Up to now the available CFD methods did not prove to be able to fulfill the industrial requirements with respect to accuracy and reliability for the aerodynamic design of helicopter main rotors. The most prominent reasons for this situation are the difficulties to provide *trimmed* CFD solutions for rotors in forward flight, the neglection of the *blade dynamics* and insufficient capabilities to account for *viscous effects*. Several researchers have tried to improve the situation with respect to consideration of blade dynamics

and included by one way or the other the elastic motion of the blades in the CFD computations.
In 1986 Tung et. al. [2] published a procedure in which the local lift coefficient or both the local lift and moment coefficients computed with a CFD method were passed to a dynamics code to calculate a new trim including blade dynamics. This so-called weak coupling approach was applied by many researchers with CFD methods which generally solve the Transonic Small Perturbation (TSP) [3] or the Full Potential equation [4]. Recently weak coupling methods have been published with an Euler [5] or a Reynolds-averaged Navier-Stokes (RANS) [6] solver on the CFD side and an elastic beam using a modal approach on the dynamics side. The comparison of the local pitching moments between Euler and N-S results in [6] clearly shows that only N-S computations are able to predict the pitching moment properly which is a prerequisite for the accurate computation of the elastic blade motion. Although the CFD method is used in a time-accurate manner the whole solution of a weak coupling method is not fully time-accurate because the fluid and the structure forces are not exactly balanced for each time step. If a fully time-accurate solution of the flow around a helicopter rotor is required a fully coupled scheme solving the fluid and the structure motion simultaneously is needed. This could be done by writing a new software package which solves the whole set of fluid and structure equations (which are descretized on different grids) as one monolithic system. Such an approach is extremely expensive in terms of software development costs. Alternatively partitioned staggered procedures were developed which make use of the best suited CFD and structure solvers by a time-accurate coupling scheme. Such staggered schemes were derived in the past by Farhat (see [7] for further references). It was proven that methods with overall 2nd order accuracy can be obtained by coupling an implicit time stepping scheme on the fluid side with an implicit scheme on the structure side (implicit/impicit scheme). In [8] and [9] iteration free implicit/impicit schemes of 2nd order accuracy are derived and applied.
In [10], [11] and [12] the inhouse flow solver INROT of the IAG ("Institut für Aerodynamik und Gasdynamik"), University of Stuttgart, is extended to RANS equations using the algebraic turbulence model of Baldwin and Lomax. The extended method is applied to hover test cases including a strong coupling with structure dynamics. The method is applied also in chimera mode for a hovering rotor and a non-lifting forward flight test case. In [13] this approach is applied to the 7A rotor in forward flight showing significant improvements compared to previous Euler results. A strong fluid-structure coupling of the DLR Euler/RANS solver FLOWer and the Eurocopter rotor dynamics code HOST is described in [14]. FLOWer/HOST computations of the inviscid flow around the ONERA 7A rotor in forward flight (μ=0.4, rotational blade tip Mach number $M_{\omega R}$ =0.656) are presented. A fully periodic solution is obtained after 8 revolutions. No trim of the CFD computations is done. The agreement of the computed with the measured normal forces is only fair which is due to the neglection of viscous effects and the fact that the CFD solution was not trimmed. Altmikus et al. present in [15] a comparison of weak and strong coupling including rotor trim based on the solution of the Euler equations. It is concluded that weak and strong coupling provide results of the same quality for steady forward flight cases (i.e. cases with periodic behaviour of the rotor blades). The comparison between measured and computed normal force and moment coefficients is again only fair although trimmed solutions are presented. One reason for this is the neglection of viscous effects which leads to false pitching moments which provide non-accurate elastic torsion deformation and hence large deviations in lift and drag at the blade tip.
Based on the literature survey given above this paper concerns itself with weakly coupled RANS solutions because this seems to be an appropriate approach to answer the industrial need for accurate simulations of rotors in forward flight. The computations in this paper include all degrees of freedom of a rotor blade (flap, lead-lag and pitching motion) if not explicitly stated differently. During the coupling procedure the normal forces, tangential forces and pitching moments are passed from the CFD solver FLOWer to the rotor simulation code S4. The progress compared to [6] is the inclusion of the lead-lag motion and the exchange of tangential forces from FLOWer to S4.

Solution Algorithm

CFD Solver FLOWer

All computations of this paper have been computed with a modified version of the block-structured DLR flow solver FLOWer [16] (Release 116.6). FLOWer is a portable software system and can be run on a large variety of computers with high efficiency. It solves the unsteady Reynolds-averaged Navier-Stokes equations, transformed into a moving blade fixed coordinate system. Details of the algorithm are given in [17]. The discretization of space and time is separated following the method of lines [18] using a cell-vertex finite volume formulation for the spatial discretization. In order to

avoid spurious oscillations, a blend of first and third order dissipative terms is introduced. Two layers of auxiliary points are used to store the neighbour flow values in order to match the solutions across inner and external cuts with second order accuracy. In the code, different turbulence models are available. In the present work only the algebraic Baldwin-Lomax model [19] with the modification of Degani and Schiff [20] is applied. The time integration uses the dual time stepping technique with a second order implicit time integration operator [21]. An important speed-up of the computations is achieved by the multigrid technique. In order to allow for elastic blade motions deforming grids are used. Free stream consistency for deforming grids is guaranteed by a geometrical conservation law [22]. At each time step the deformed blade surface is computed using a Fourier series for each of the blade mode shapes which was calculated with the rotor simulation code S4. The deformed volume grid is then generated using transfinite interpolation techniques. The method is independent of the block topology and can also be applied to multiblock cases. The grid quality close to the blade is of the same quality as the undeformed grid. For highly distorted grids the quality of the grid at inner cuts may be only fair.

Rotor Simulation Code S4

The DLR rotor simulation code S4 originally was developed to compute effects of Higher Harmonic Control (HHC) onto dynamic rotor forces of a hingeless rotor in the nonrotating frame [23], [24]. With time, it evolved into a comprehensive code for the computation of isolated rotors with high resolution blade loads for acoustic postprocessing. It is validated by studies about active control of HHC or Individual Blade Control (IBC) [25], and the effects of dynamic stall[26]. It mainly consists of 3 modules:
The aerodynamics, the structural dynamics and the induced velocities module. They are embedded in a trim algorithm and comprise:

- The aerodynamic module [27]-[29], with nonlinear unsteady aerodynamics (incl. Mach effects, dynamic stall, varying velocity effects and yaw influence). The blade is discretized into 20 elements of decreasing size radially. In each of them, the time histories of Mach numbers at the collocation point (located at three-quarter chord) are computed, which form the basis input of the unsteady aerodynamics computation. The local forces and moments are summed up into the generalized modal forces of the respective blade modes.
- The structural dynamics module represents an arbitrary number of articulated or hingeless elastic blades. Each blade is represented by its mode shapes and natural frequencies in flap, lead-lag and torsion separately. Both the mode shapes and the natural frequencies are taken from either experiments or -usually- from a finite element computation. Within the rotor code, the generalized coordinates of each mode are computed by time integration of their differential equations of motion, having the generalized aerodynamic forcing on the right hand side of the equations. For this purpose, a Runge-Kutta 4^{th} order scheme is used.
- The third important module is associated with the induced velocities. For this study, a prescribed tip vortex wake [30] is used, together with rotor-body interactions and wind tunnel-body interactions [31].

The overall handling is done with an automatic trim module for specified non-rotating hub forces and moments. As degrees of freedom to trim to the desired values, the collective and cyclic controls are used; and in addition the rotor shaft angle of attack is taken. The rotor trim is defined by measured values of vertical and propulsive forces, plus pitch and roll moment, and the wind tunnel data like temperature, pressure, and velocity.

Coupling Procedure for Weak Coupling

The coupling between the CFD method FLOWer and the rotor simulation code S4 is carried out as follows (see Figure 1). First a trim computation is carried out with S4 alone. After this trim computation the elastic blade motion based on the aerodynamic forces of the blade element theory is known. The CFD code is then applied with this prescribed blade motion including an elastic motion of the blade and provides a field of aerodynamic forces and moments for each blade element and each azimuth position.

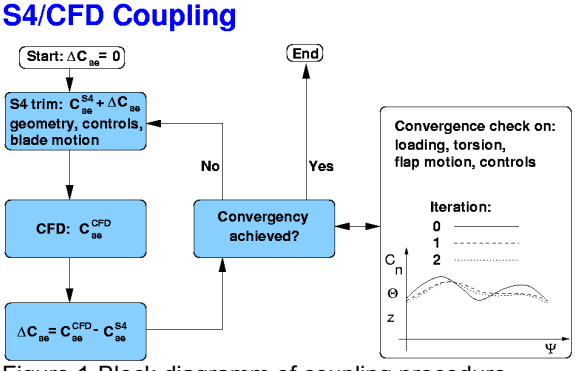

Figure 1 Block diagramm of coupling procedure

The difference between the CFD aerodynamics and the S4 aerodynamics is computed. This difference is added to the S4 aerodynamic model in terms of normal forces (c_nM^2), tangential forces (c_tM^2) *and* moments (c_mM^2) for the next iteration (see Figure 1). The new trim is now obtained based on the S4 aerodynamics plus the difference to the CFD aerodynamics. This procedure is repeated until the blade motion (control angles, rotor shaft angle and elastic blade motion) between two consecutive iterations is below a certain threshold.

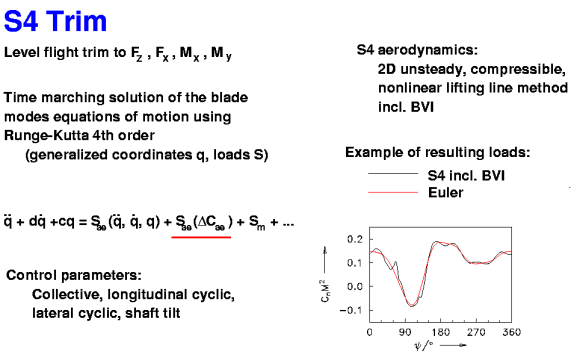

Figure 2 Trim procedure of the S4 code

By this coupling method the equation of motion of the rotor blade is solved with the aerodynamic forces computed with the CFD method if the iteration process converges. In the isolated blade computations the blade wake can only be computed inside the CFD grid. When complete rotors are computed (even with the chimera method), the individual vortices are diffused due to numerical dissipation as a consequence of the coarseness of the CFD grids some chords away from the blade. This problem is associated with a loss of blade-vortex interaction (BVI) effects, and is overcome by the following procedure: The CFD results contain harmonics usually up to 6/rev, with rather small amplitudes in the frequencies above 6/rev.Therefore the CFD results are low-pass filtered at 6/rev, and the same is done with the S4 loads, which do include BVI due to the prescribed wake used. An aerodynamic difference matrix is computed for this low frequency content (e.g. Δc_nM^2 = c_nM^2(CFD) - c_nM^2(S4)) and added to the next S4 trim as a non-variable aerodynamic offset. Thus, after convergence is obtained, the first 6 harmonics represent exactly the CFD aerodynamics, and all higher harmonics include BVI effects from S4, which are not contained in the CFD results.

Test Cases

High-speed forward flight test cases of the fully articulated 4-bladed ONERA 7A and 7AD rotors were selected. The 7A and the 7AD rotors are fully instrumented rotors which were designed by ECF and tested in the ONERA S1 wind tunnel at the Modane test center (see [32]). The 7A rotor has rectangular blades whereas the 7AD rotor has a parabolic swept back tip with anhedral and a straight trailing edge. Both rotors have an aspect ratio of R/c_{root}=15. The test cases chosen correspond to a rotational tip speed Mach number of $M_{\omega R}$=0.64 with an advance ratio of μ=0.4, a lift coefficient of Zb=12.56 and a propulsive force coefficient of Xb=1.6. Chordwise pressure distributions were measured at 5 spanwise stations (0.5R, 0.7R, 0.825R, 0.915R, 0.975R). The integration of these pressures is used to compute the experimental normal force coefficients and pitching moments at these stations.

Grid Generation

Grids were generated for two different approaches: single block grids around isolated blades and a multiblock chimera grid around the whole 7A rotor.
An isolated blade computation means that only the near wake is part of the solution. The downwash of the other blades is not accounted for. This simplification was done in order to reduce the computational effort, knowing that this will reduce the accuracy of the solution. As the selected test case is a high-speed forward flight case, an acceptable agreement of the computational results close to the blade tip with the experimental data can be expected, because the effect of the induced velocities is comparably small at the blade tip for such high-speed cases (except where BVI occurs). The vortical wake system is part of the solution in the case of the chimera computation.

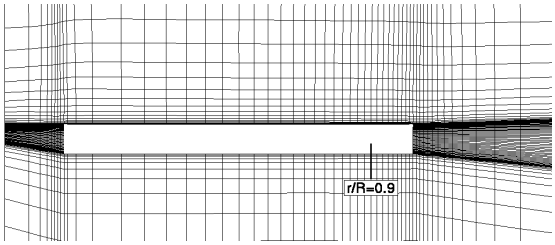

Figure 3 Isolated blade grid in rotor plane (7A)

The grids are of CH type and were generated as follows. First a set of 2d grids around each blade section was generated using an algebraic grid generator. This set was staggered to form a 3d grid which was 3d elliptically smoothed [33], [34]. A boundary layer grid was splined into the 3d grid. The grid around the 7A rotor blade in the rotor plane is shown in Figure 3 while the grid at r/R=0.9 is presented in Figure 4. In Figure 5 the grid in the rotor plane of the 7AD rotor is plotted. Please note the parabolic swept

back tip of the 7AD rotor. The grids around isolated blades have a farfield distance of 20 chords referred to the chord length at the blade root (r/R=0.2).

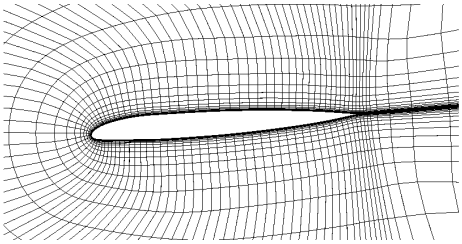

Figure 4 Grid section at r/R=0.9

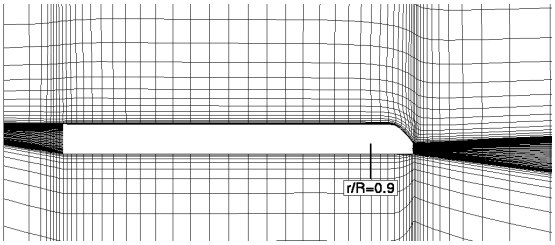

Figure 5 Isolated blade grid in rotor plane (7AD)

The child grids for the chimera grid system around the 7A rotor were generated in the same manner as the grids around isolated blades except that the distance from the blade surface to the outer boundary of the child grids is about 3c. The farfield distance is at minimum 1R in all directions. A cartesian background grid with non-aequidistant spacing was used (see Figure 6, only every other grid point printed).

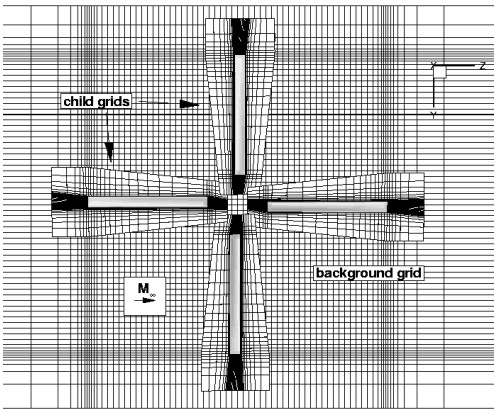

Figure 6 Top view of chimera grid system (7A)

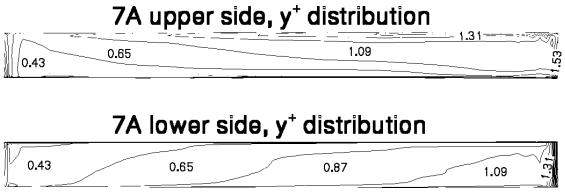

Figure 7 y+-distribution on the blade surface (7A rotor)

Figure 7 shows the y^+-distribution of the first grid points normal to the wall for the 7A rotor at $\psi=0^o$. The first grid spacing was set to 1.5e-5 c_{root} which corresponds to y^+-values of about 1 for a Reynolds number of about 2e+6. The most part of the blade has y^+-values which are around 1. At the very leading edge on the upper side y^+-values up to 2.5 are reached between r/R=0.7 and r/R=1.0. Only in the last row of cells at the very tip the y^+-values are between 2.5 and 3.5. This distribution of y^+-values is acceptable for resolving the high velocity gradients close to the blade surface. Still it should be kept in mind that this grid has only about 17 cells in the boundary layer which reproduces the main viscous effects but which cannot give a fully grid converged flow solution in the boundary layer. The flow was assumed to be fully turbulent.
The grid dimensions are:

Table 1: Number of grid cells

				Cells on blade surface		
	I	J	K	I	K	Total
isol. bl.	128	40	56	96	32	286 720
Chimera Child	144	48	68	96	48	470 016
Chimera Back-ground	64	144	144			1.3 e6
Chimera total						3.2 e6

The blade descretization for the S4 code consists of 20 blade elements with a reduced element size close to the blade tip. Further details on the blade discretization are given in Figure 8 and Table 1. The I-direction corresponds to the wrap-around direction, the J-direction to the direction normal to the blade surface and the K-direction to the radial direction.

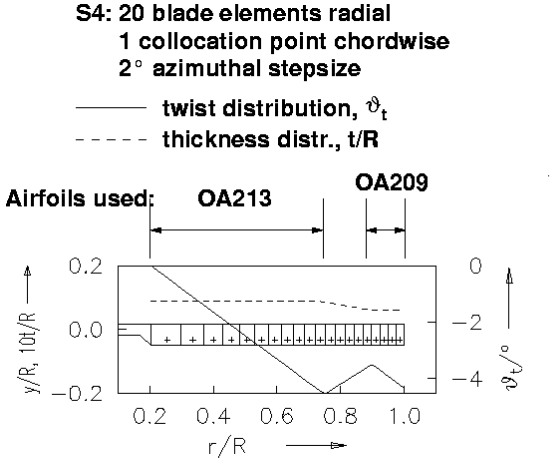

Figure 8 Blade discretization for S4

Results

Comparison of Isolated Blade and Multiblade Computations for the 7A Rotor and c_n+c_m-Coupling

In this chapter results will be presented which compare isolated blade and multiblade computations (chimera technique) using a coupling which transfers only the normal forces and pitching moments (c_n+c_m-coupling) but not the tangential forces from the CFD code FLOWer to the rotor simulation code S4. The lead-lag motion was neglected for the computations to be presented in this chapter. Due to a misunderstanding the trim for these computations was not carried out for Xb=1.6 but for Xb=2.17 which is considerably higher. Therefore no comparison with experimental data is shown in this chapter. Still the results obtained for this trim can serve as an example of the differences between isolated blade and multiblade computations.

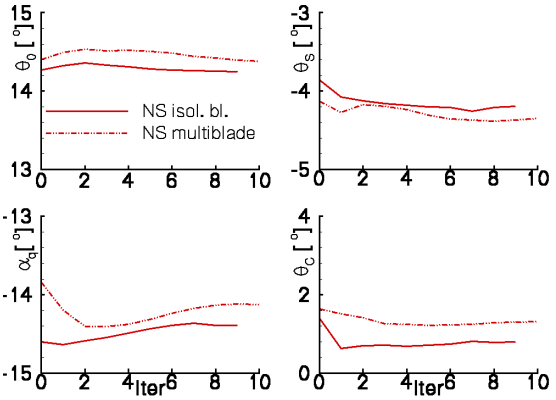

Figure 9 Convergence of control angles and shaft angle (7A rotor, c_n+c_m-coupling)

With respect to the convergence of the coupling procedure it can be seen in Figure 9 that the chimera computation needs more coupling iterations to converge. In fact 9 Iterations are needed whereas the isolated blade computation is converged after 6-7 iterations. An increase for the multibladed computation when compared to the isolated blade run in α_q, θ_0, and θ_C of about 0.2° can be noted. θ_S is slightly lower for the multibladed computation. These changes in controls are due to the missing vortical wake of the other blades in the isolated blade computation. Generally speaking these differences in trim condition are small. This shows that for such a high-speed test case the wake is quickly convected downwards which produces relatively small induced velocities on the rotor blades.

The comparison of the normal forces and the pitching moment distributions in Figure 10 and Figure 11 shows relatively small differences between the isolated blade and the multiblade (chimera) computations. But it should be noted that the effect of the wake which is computed in the chimera computation reduces the negative peak in the normal forces around 120° azimuth, moves the negative peak slightly to higher azimuth values and makes the descent to the minimum c_nM^2-values steeper. Additionally it is worth to be mentioned that the chimera method computes a pitching moment distribution (see Figure 11) which shows a double peak pattern for r/R=0.825 around ψ=90° which is not the case for the isolated blade computation.

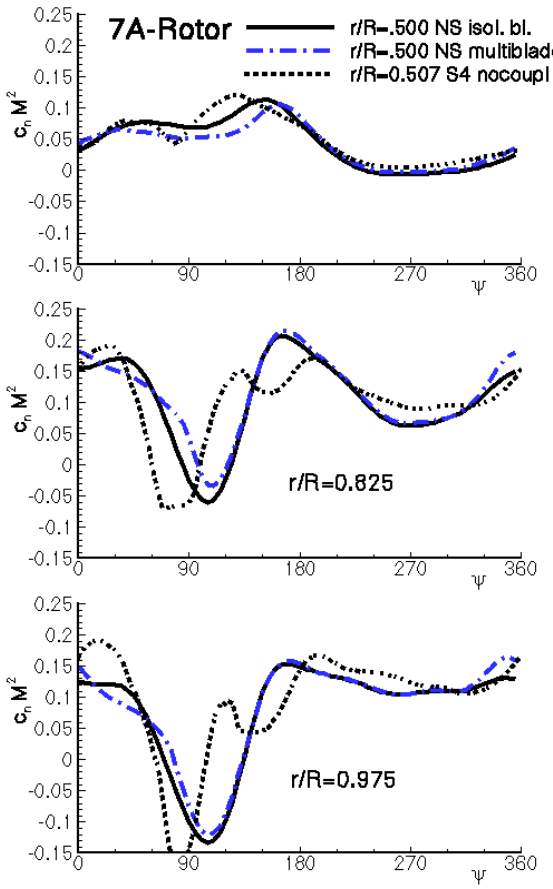

Figure 10 Normal force distributions of the coupled isolated blade, the multiblade and the uncoupled S4 computations (7A rotor, c_n+c_m-coupling)

Figure 12 presents the elastic torsion deformation at the blade tip of the two computations. The chimera computation shows a minimum torsion angle of about –2.2° while the isolated blade computation computes a minimum elastic torsion of only -1.8°. The 5th harmonic content which is obvious in the chimera computation cannot be seen in the isolated blade results.

Figure 13 compares the normal force distributions for isolated blade computations with cn+cm- and cn+ct+cm-coupling. There is a

large difference between the two solutions which shows the importance to include the tangential forces in the coupling process.

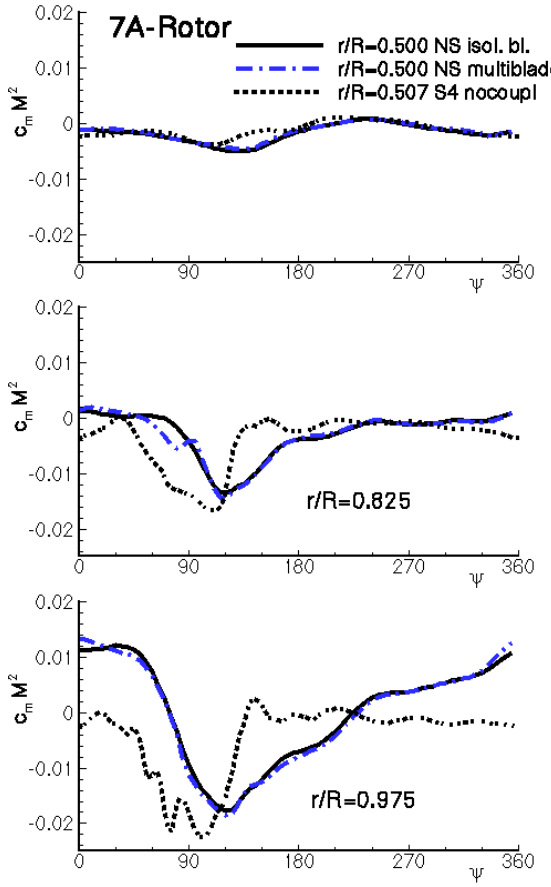

Figure 11 Moment distributions of the coupled mono block, the chimera Navier-Stokes and the uncoupled S4 computations

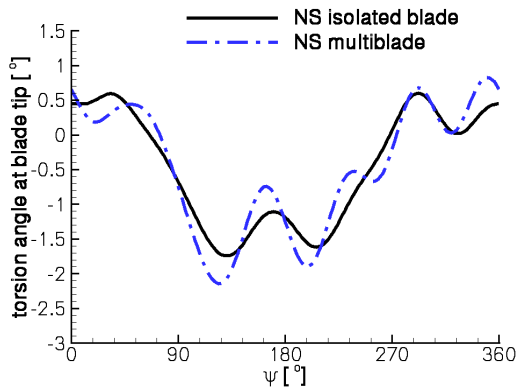

Figure 12 Elastic torsion at the blade tip (7A rotor, c_n+c_m-coupling)

These observations are consistent with the investigation in [5] where it was concluded that only a coupling which includes lift, drag and moment will provide a solution which is independent of the simplified aerodynamics of the rotor simulation code which was applied in the coupling procedure. This large effect of the tangential forces may be surprising because the tangential forces are about one order of magnitude smaller than the normal forces. But on the other hand it should be kept in mind that the propulsive force of the main rotor of a classical helicopter is roughly one order of magnitude smaller than the lift force. Every parameter with an effect on the propulsive force will therefore strongly effect the trim condition of the rotor (especially the shaft angle) which has a direct effect on the power consumption in order to maintain certain values of lift and propulsive force (Zb and Xb).

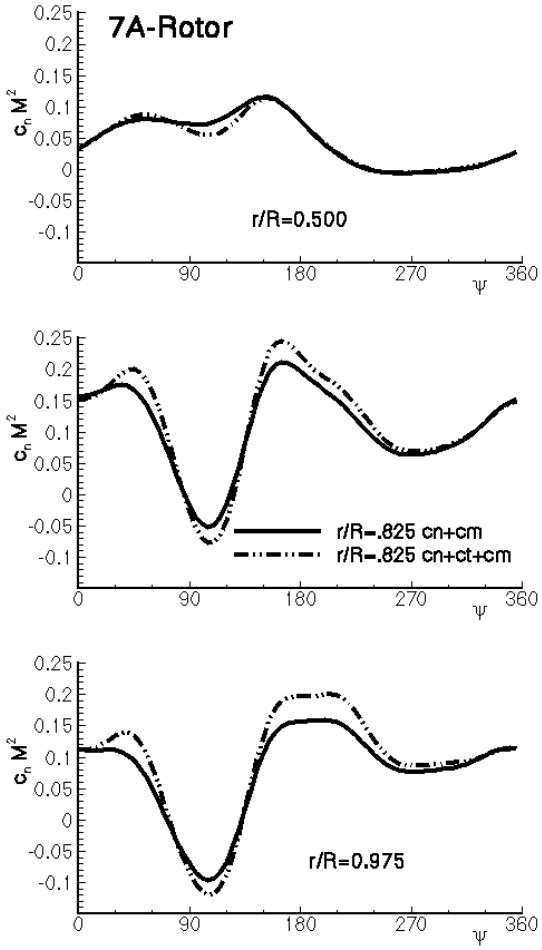

Figure 13 Normal force distributions of the isolated blade computations with c_n+c_m- and c_n+c_t+c_m-coupling (7A rotor, Xb=2.17)

Isolated Blade Computation for the 7A Rotor with c_n+c_t+c_m-Coupling

The results of this chapter have been obtained applying a trim which meets Xb=1.6, Zb=12.56, the rolling and the pitching moment of the wind tunnel test. The trim was not done in order to obey the so called modane law (Xb, Zb, β_S=0, β_C=-θ_S) but in order to meet the forces and moments. The lead-lag motion is accounted for in the following.

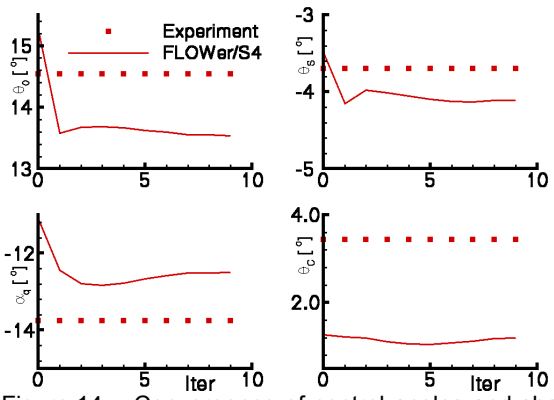

Figure 14 Convergence of control angles and shaft angle (7A rotor)

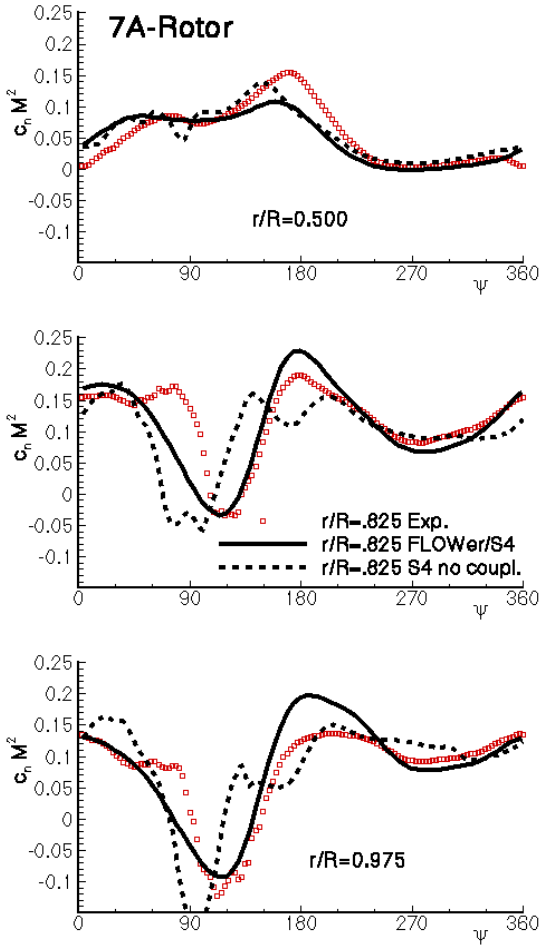

Figure 15 Normal forces distributions for the coupled N-S und the uncoupled S4 computations (7A rotor)

Figure 14 shows the convergence of the control angles (θ_0, θ_S, θ_C) and the shaft angle α_q for the coupled 7A computations. The corresponding experimental values are given as square symbols. The computations were accepted as converged when the changes of the control angles and the shaft angle between two consecutive iterations was below 0.04°. The computation needed 8 iterations to converge.

The largest differences between the computed control angles/shaft angle and the measured ones of more than 2° are observed for the control angle θ_C. The shaft angle and the other control angles show differences of up to 1.0°, which is only a fair agreement.

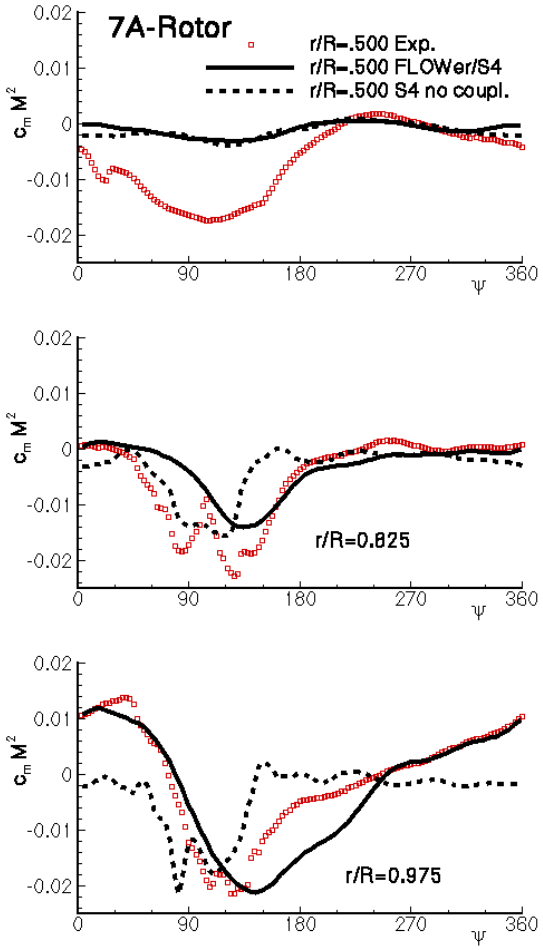

Figure 16 Moment distributions for the coupled N-S und the uncoupled S4 computations (7A rotor)

A comparison of the normal force distributions for the uncoupled S4 and the coupled FLOWer/S4 computations with the experimental data is presented in Figure 15. The numerical prediction is qualitatively in good agreement with the experimental data. The strong negative peak in the normal forces is well captured by the coupled FLOWer/S4 computation although it has to be stated that the difference between the minimum and the maximum c_nM^2 values is over predicted. Looking to the pitching moments (c_mM^2) in Figure 16 a fair agreement between the coupled computation and the measurements is achieved for r>0.8R. For r/R=0.5 the prediction agrees only poorly with the measured data. The comparison of the results for the un-

coupled S4 computation and the coupled FLOWer/S4 computations shows a clear improvement in the overall shape of the c_nM^2- or c_mM^2-curves and especially in the phase when compared with the experimental data. It should be kept in mind that these results were obtained with isolated blade computations only and can therefore not contain any kind of blade vortex or blade wake interaction. It can be expected that a multiblade computation with the chimera scheme will modify the solution in a similar way as it was described in the previous chapter. A very good comparison for the c_nM^2-values and a good one for the c_mM^2-values with the measured data can be expected in this case.

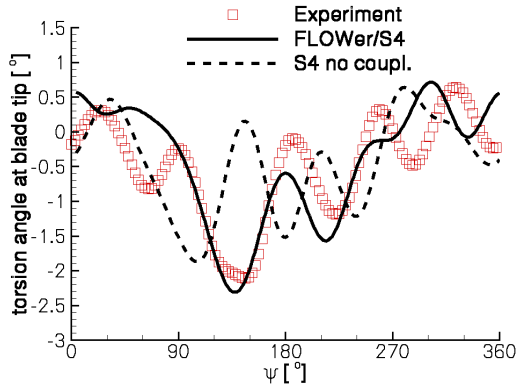

Figure 17 Elastic torsion at the blade tip (7A rotor)

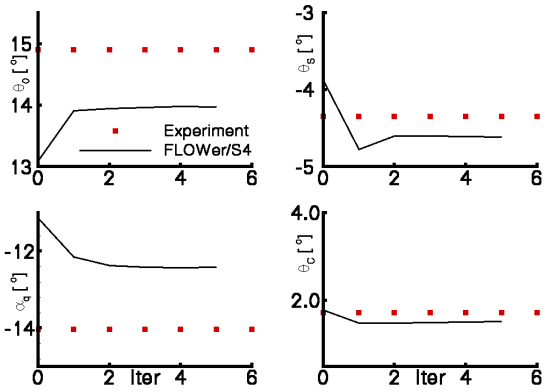

Figure 18 Convergence of control angles and shaft angle (7AD rotor)

The elastic torsion at the blade tip is plotted in Figure 17. The maximum elastic torsion of about –2.2° is well captured. When comparing the uncoupled S4 solution with the coupled FLOWer/S4 solution it is obvious that the S4 solution shows a considerable 5/rev content as it is seen in the experimental data and as it was also computed with the multibladed computation (see Figure 10) whereas the coupled FLOWer/S4 computation shows only a very small 5/rev content. The reason for this difference is the missing rotor wake system in the isolated blade computation. The 5/rev motion is obviously excited by an interaction of the blade with the rotor wake system.

Isolated Blade Computation for the 7AD Rotor with c_n+c_t+c_m-Coupling

In this chapter the results of isolated blade computations for the 7AD rotor with c_n+c_t+c_m-coupling are presented and discussed.

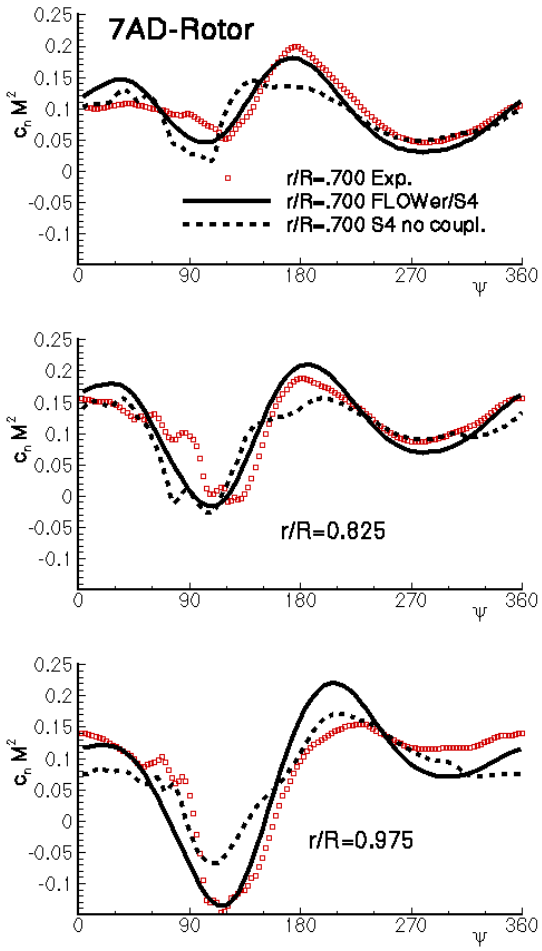

Figure 19 Normal force distributions for the coupled NS und the uncoupled S4 computations (7AD rotor)

The convergence of the control angles (θ_0, θ_S, θ_C) and the shaft angle α_q for the coupled 7AD computations is depicted in Figure 18. The corresponding experimental values are given as square symbols. The computations were accepted as converged when the changes of the control angles and the shaft angle between two consecutive iterations was below 0.04°. The computation needed 4 iterations to converge which is considerably faster than the computations for the 7A rotor. The lateral and the longitudinal control is in excellent agreement with the experimental data while the computed collective differs from the measured one by 1° and the difference in the shaft angle is about 1.5°. As in the 7A case the predicted absolute values of the

shaft angle and the collective control angle are smaller than the corresponding experimental data.

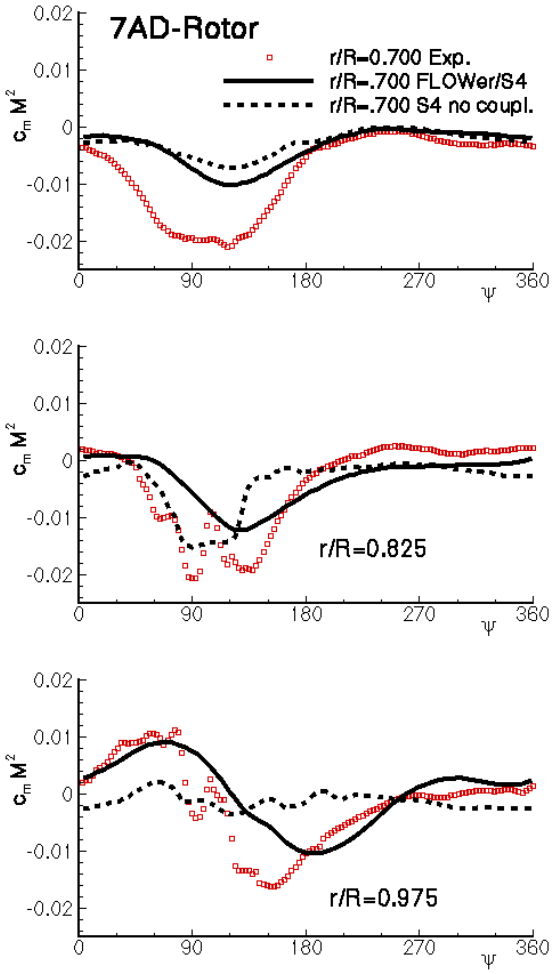

Figure 20 Moment distributions for the coupled NS und the uncoupled S4 computations (7AD rotor)

Figure 19 shows the normal force distributions for r/R=0.7, 0.825 and 0.975. The section at r/R=0.7 was chosen as the most inboard section because no experimental data was available for this test case at r/R=0.5. The overall agreement between predicted and measured normal forces in Figure 19 is good. The phase and the negative peak in the normal forces are well reproduced by the simulation. The comparison of the uncoupled S4 with the coupled FLOWer/S4 computation and the experimental data shows first of all that the S4 code with its simplified aerodynamics performs very well. Further the coupled solution is able to predict the negative peak in the normal forces around 120° azimuth better. In the uncoupled S4 computation which uses a prescribed wake model a clear interaction of the blade with the vortical wake is predicted for $60° < \psi < 100°$ which corresponds to the effects in the wind tunnel data. These effects are not included in the isolated blade computations as explained before. This is why the agreement between the coupled Navier-Stokes solution and the experimental data is less good in this azimuth region. The computed and measured pitching moments are compared in Figure 20. The agreement between prediction and measurement is comparable to the results of the 7A rotor. Similar comments as for the normal forces hold when comparing the uncoupled S4 computation with the coupled FLOWer/S4 computation. A double peak pattern is seen in the experimental data for the pitching moment at r/R=0.825 and for this case also for r/R=0.975. This pattern is not reproduced by the simulation. Since a weak double peak pattern was found for the multibladed (chimera) computation with c_n+c_m coupling it is hoped that a chimera computation would improve the results.

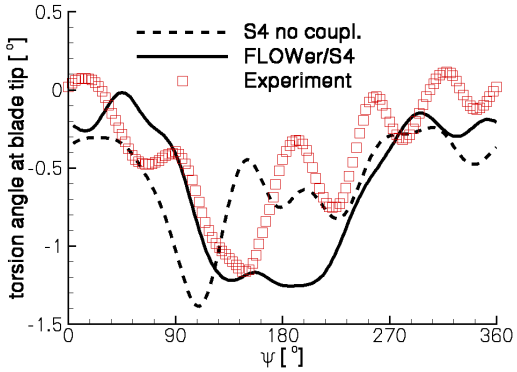

Figure 21 Elastic torsion at the blade tip (7AD)

The elastic blade torsion is given in Figure 21. The blade torsion computed with the weak coupling of FLOWer and S4 does not show a 5/rev content whereas the uncoupled S4 computation does. The reason for this is the same as in the 7A case. The 5/rev content of the elastic torsion at the blade tip for the 7AD rotor is much smaller than for the 7A rotor. There are two reasons for this. One is the different aerodynamic behaviour of the two rotors. The 7AD rotor produces considerably lower pitching moments at the blade tip with a strong aerodynamic damping because of the planform which results in a lower excitation of 5 or 6/rev elastic torsion motions. Additionally the 7AD rotor has a torsional Eigenfrequency which is between 6 and 7/rev while the Eigenfrequency of the 7A rotor is almost exactly 6/rev. Therefore elastic oscillations are more easily excited in the case of the 7A rotor. This is in fact also the reason for the different convergence behaviour of the weakly coupled computations for the two rotors. The large number of iterations for the 7A rotor is needed in order to converge the elastic torsion

which takes much longer in the case of the 7A rotor because of its low aerodynamic damping.

Synthesis of 7A and 7AD results

The weak coupling with normal forces, tangential forces and pitching moments based on Navier-Stokes computations predicted the normal force distributions quite well. The predicted moments showed for both rotors considerable differences to the experimental data for r/R=0.5/0.7. The agreement of predicted and measured moments close to the blade tip was quite good.

Table 2: Computational Effort

Description	Rotor	CPU-Time [h]/Rev on 1 Proc. NEC-SX5
N-S	7A	3:30
N-S chimera	7A	49:15
N-S	7AD	3:30

The computational effort is given in Table 2. For this kind of application which includes deforming meshes and chimera functionalities a performance of only 1 GFLOPS is obtained on one processor of the DLR NEC-SX5. The reason for this poor performance is that the chimera search and most parts of the grid deformation tool in FLOWer 116.6 are not well vectorized. Modified modules have been developed but they arrived to late to be included in this investigation.

The predicted and measured power consumption of the 7A and the 7AD rotor are presented in Figure 22. All power evaluations were done within the S4 code and only the coupling with isolated blade CFD computations was considered since no coupled chimera results were available for this trim. The S4 code alone underpredicts the power consumption by 23.6% for the 7A and 21.2% for the 7AD rotor whereas the coupled computations overpredict the absolute power consumption by 16.9% for the 7A and 16.2% for the 7AD rotor. The agreement between simulation and measurement for the absolute values is improved by the weak coupling although the agreement is not satisfactory. But this had to be expected for the following reasons. The effect of transition from laminar to turbulent boundary layer was not considered in this computation. This effect will reduce the rotor power by several percent (about 5% were obtained for the 7A rotor in hover in [35]). The blade stubs were not gridded for this investigation (see Figure 3) which produces a too strong vortex at the blade root. A reduction in power of about 4-5% when accounting for the blade stubs can be expected. Finally it is recalled that the computations where carried out with an algebraic turbulence model on grids around isolated blades with only a medium grid point density. Still it may be assumed that the aforementioned effects will modify the predictions for the two rotors similarly. When the prediction of the power difference between the two rotors is compared a considerable improvement because of the weak coupling can be observed. With the weak coupling a reduction in power consumption when comparing the 7AD and the 7A rotor of about 6.0% (7.2 kW) is predicted which compares well to the measured 5.5% (5.6 kW) reduction.

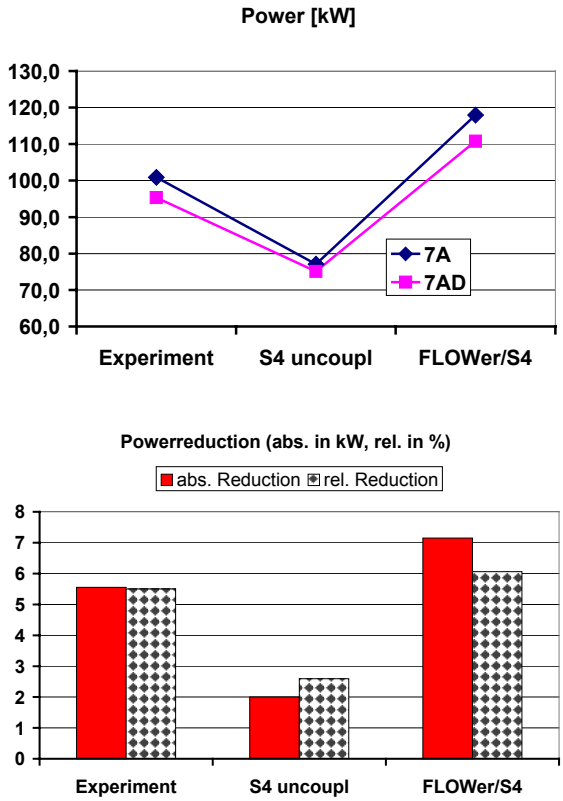

Figure 22 Power for 7A and 7AD rotor and power difference between these rotors

Conclusion and Future Activities

A weak coupling procedure for coupling the rotor simulation code S4 and the Euler/Navier-Stokes solver FLOWer which exchanged only the local normal forces and pitching moments was extended to include also the tangential forces for the data transfer from the CFD method to the rotor simulation code. The method allows to produce trimmed CFD solutions for rotors in high-speed forward flight accounting for elastic blade deformations and viscous effects. The weak coupling procedure was applied to high-speed forward flight test cases of the 7A and the 7AD rotor. Isolated

blade computations were carried out for both rotors while a chimera computation around the whole 4-bladed rotor was carried out only for the 7A rotor. A clear improvement of the solution with respect to the existing experimental data because of the weak coupling was proven. The well known negative peak in the normal forces distribution close to the blade tip around 90^o-120^o for elastic blades in high-speed forward flight was well reproduced with the coupled Navier-Stokes computations. Even the phase agrees well.
Although the evaluation presented in this paper was based on isolated blade computations only it was able to predict the performance differences between the 7A and the 7AD rotor in high-speed forward flight well although the absolute power was overpredicted for both rotors by about 17%.
With respect to the coupling procedure it can be concluded that on the CFD side a method which includes viscous effects is mandatory and only a coupling with normal forces, tangential forces and pitching moments makes good sense.

The next steps will be to carry out chimera computations for both rotors. Then the method has to be applied to other flight conditions. A procedure has to be developed which allows to account for the laminar/turbulent transition. Furthermore the coupling will also be done with the Eurocopter standard tool HOST.
For an industrial application the user workload has to be considerably reduced by automatization of the coupling procedure. Furthermore a significant reduction of the computational effort is required.

References

[1] Toulmay, F.: „Rotorcraft Aerodynamics: Challenges, Perspectives and Priorities“, CEAS Aerospace Aerodynamics Conference, 10-12 June 2002, Combridge UK.

[2] Tung, C., Caradonna, F.X., Johnson, W.: *The Prediction of Transonic Flow on an Advancing Rotor*. Journal of the American Helicopter Society, Vol. 31, No 3, July 1986, pp 4-9.

[3] Desopper, A., Chopra, I., Kim, K.C.: *Dynamic Blade Response Calculations using Improved Aerodynamic Modeling*. National Specialists' Meeting on Aerodynamics and Acoustics, Fort Worth, Texas, February 1987.

[4] Beaumier, P.: *A Coupling Procedure between a Rotor Dynamics Code and a 3D Unsteady Full Potential Code*. American Helicopter Society Aeromechanics Specialists Conference, San Francisco, California, January 1994.

[5] Servera, G.; Beaumier, Ph.; Costes, M.*: A weak coupling method between the Dynamics code HOST and the 3D Unsteady Euler code WAVES*. 26th ERF Forum, Sept. 2000.

[6] Pahlke, K.; Van der Wall, B.: *Calculation of Multibladed Rotors in High-Speed Forward Flight with weak Fluid-Structure-Coupling*. 27th European Rotorcraft Forum, Moscow, Sept.11-14, 2001.

[7] Farhat, C.: *High Performance Simulation of Coupled Nonlinear Transient Aeroelastic problems*. AGARD R-807.

[8] Hierholz, K.-H. and Wagner, S.: *Simulation of Fluid Structure Interaction at the Helicopter Rotor*. Proceedings of the 21st ICAS Congress, Melbourne, Australias, Spet. 13-18, ICAS-98-2.9.4, 1998.

[9] Hierholz, K.-H.: Ein numerisches Verfahren zur Simulation der Strömungs-Struktur-Interaktion am Hubschrauberrotor. Ph.-D. Thesis, Institut für Aerodynamik und Gasdynamik, Universität Stuttgart, 1999.

[10] Pomin, H. and Wagner, S.: *Navier-Stokes Analysis of Isolated Rotor Flow in Helicopter Hover Flight*. Proceedings: European Congress on Computational Methods in Applied Sciences and Engineering (ECCOMAS), Barcelona/Catalonia, September 11-14, 2000.

[11] Pomin, H., Altmikus, A., Buchtala, B. and Wagner, S.: *Rotary Wing Aerodynamics and Aeroelasticity*. In: High Performance Computing in Science and Engineering 2000. E. Krause and W. Jäger (Eds.), pp. 338-348, Springer-Verlag, Berlin, Heidelberg, 2001.

[12] Pomin, H. and Wagner, S*.: Navier-Stokes Analysis of Helicopter Rotor Aerodynamics in Hover and Forward Flight*. AIAA-Paper 2001-0998, 39th AIAA Aerospace Sciences Meeting & Exhibit, Reno/Nevada, January 8-11, 2001.

[13] Pomin, H. and Wagner, S*.: Aeroelastic Analysis of Helicopter Rotor Blades on Deformable Chimera Grids*. AIAA-Paper 2002-0951, 40th AIAA Aerospace Sciences Meeting & Exhibit, Reno/Nevada, January 14-17, 2002.

[14] Altmikus, A. R. M. and Wagner, S*.: On the Accuracy of Aeroelastic Simulations of Rotary Wings*. AHS Aerodynamics, Acoustics and Test and Evaluation Technical Specialist Meeting, San Franscisco, CA, January 2002.

[15] Altmikus, A. R. M.; Wagner, S.; Beaumier, P. and Servera, G.: „A Comparison: Weak vs Strong Modular Coupling for Trimmed Aeroelastic Rotor Simulations“, 58th AHS Forum, Montreal, Canada, June 11-13, 2002.

[16] Kroll, N.; Rossow, C.C.; Becker, K. and Thiele, F.: “MEGAFLOW-A Numerical Flow Simulation system“, ICAS-congress, September 1998, Melbourne, Australia.

[17] Pahlke,K.: “Berechnung von Strömungsfeldern um Hubschrauberrotoren im Vorwärtsflug durch die Lösung der Euler-Gleichungen“, DLR-Forschungsbericht 1999-22, ISSN 1434-8454, 1999.

[18] Jameson, A.; Schmidt, W. and Turkel, E.: “Numerical Solutions of the Euler Equations by Finite Volume Methods Using Runge-Kutta Time-Stepping Schemes“, AIAA Paper 81-1259, 1981

[19] Baldwin, B. and Lomax, H., "Thin Layer Approximation and Algebraic Model For Separated Turbulent Flows", AIAA-Paper 78-0257,197
[20] Degani and Schiff, L., "Computation of Turbulent Supersonic Flows around Pointed Bodies having Crossflow Separation", Journal of Computational Physics Vol. 66, pp. 176-196, 1986.
[21] Jameson, A.: „Time Dependent Calculation Using Multigrid, with Applications to Unsteady Flows Past Airfoils and Wings“, AIAA Paper 91-1596, 1991.
[22] Gaitonde, A. L. and Fiddes, S.: „A Three-Dimensional Moving Mesh Method for the Calculation of Unsteady Transonic Flows“, University of Bristol, Rep. No. 483, Sept. 1993.
[23] van der Wall, B. G.: "An Analytical Model of Unsteady Profile Aerodynamics and its Application to a Rotor Simulation Program", 15th European Rotorcraft Forum, Amsterdam, Netherlands, 1989.,
[24] van der Wall, B. G.: "Analytic Formulation of Unsteady Profile Aerodynamics and its Application to Simulation of Rotors", DLR-FB 90-28, 1990, also: ESA-Report No. ESA-TT-1244, 1992.
[25] Beaumier, P.; Prieur, J.; Rahier, G.; Spiegel, P.; Demargne, A.; Tung, C.; Gallmann, J.M.; Yu, Y.; Kube, R.; van der Wall, B.G.; Schultz, K.J.; Splettstoesser, W.R.; Brooks, T.F.; Burley, C.L.; Boyd, D.D.: "Effect of Higher Harmonic Control on Helicopter Rotor Blade-Vortex Interaction Noise: Prediction and Initial Validation", AGARD-CP-552, 1995; also: 75th Fluid Dynamics Symposium, Berlin, Germany, 1994
[26] Petot, D.; Arnaud, G.; Harrison, R.; Stevens, J.; Teves, D.; van der Wall, B.G.; Young, C. and Széchényi, E.: "Stall Effects and Blade Torsion - an Evaluation of Predictive Tools", 23rd European Rotorcraft Forum, Dresden, Germany, 1997.
[27] Leiss, U.: "A Consistent Mathematical Model to Simulate Steady and Unsteady Rotor-Blade Aerodynamics", 10th European Rotorcraft Forum, Den Haag, Netherlands, 1984.
[28] Leiss,U.: "Unsteady Sweep - A key to Simulation of Threedimensional Rotor Blade Airloads", 11th European Rotorcraft Forum, London, England, 1985.
[29] van der Wall, B.G. and Leishman, J.G.: "On the Influence of Time-Varying Flow Velocity on Unsteady Aerodynamics", Journal of the American Helicopter Society, Vol. 39, Nr. 4, 1994.
[30] van der Wall, B.G.: "Simulation of HHC on Helicopter Rotor BVI Noise Emission using a Prescribed Wake Method", 26th European Rotorcraft Forum, The Hague, Netherlands, 2000.
[31] Goepel, C. and van der Wall, B.G.: "Berechnung der induzierten Geschwindigkeiten des Rotorversuchsstandes ROTEST im DNW", DLR IB 111-89/27, 1989.
[32] Beaumier, P.; Costes, M. and Gavériaux, R.: "Comparison Between FP3D full Potential Calculations and S1 Modane Wind Tunnel Test Results on Advanced Fully Instrumented Rotors" 19th ERF, Cernobbio, Como (Italy), Sept. 1993.
[33] O. Brodersen,O.; M. Hepperle, M.; Ronzheimer, A.; Rossow, C.-C. and Schöning, B.: „The Parametric Grid Generation System MegaCads“, Proc. of 5th International Conference on Numerical Grid Generation in Computational Field Simulation, Ed. B.K. Soni et.al., 1996, 353—362.
[34] Brodersen, O.; Ronzheimer, A.; Ziegler, R.; Kunert, T.; Wild, J. and Hepperle, M.: „Aerodynamic Applications using MegaCads“, Proc. of 6th International Conference on Numerical Grid Generation in Computational Field Simulation, Editor M. Cross et.al., 1998, 793—802.
[35] Beaumier, P.; Chelli, E. and Pahlke, K. “Navier-Stokes Prediction of Helicopter Rotor Performance in Hover Including Aero-Elastic Effects”, 56th AHS Forum, May 2-4, 2000.